Rate-Splitting Multiple Access for Satellite Short-Packet Communications: Finite Blocklength Modeling and Reliability Analysis

Sang-Quang Nguyen[(1)(*)], and Chi-Bao Le[(2)]

***Abstract*—Short-packet transmission is becoming crucial for satellite services that cannot rely on long codewords to hit the required latency and reliability. This study investigates rate-splitting multiple access (RSMA) in that context and builds a finite-blocklength (FBL) model for a downlink satellite-terrestrial link affected by Shadowed-Rician fading. We obtain closed-form approximations for the block error rate (BLER) of both the common and private streams, explicitly incorporating imperfect successive interference cancellation (ipSIC) at the receivers. Compared with power-domain non-orthogonal multiple access (NOMA), RSMA exhibits more stable BLER the common stream helps dampen residual interference due to ipSIC and the short-packet effect–so RSMA generally needs less transmit power to attain the same error targets. Numerical results validate the analysis and demonstrate consistent RSMA advantages across a wide range of transmit powers, blocklengths, shadowing severities, and antenna configurations. The results suggest that RSMA is a very promising option for future satellite systems that need to provide reliable, low-latency, and short-packet communications in view of realistic SIC imperfections.**

***Index Terms*—Rate-splitting multiple access, finite blocklength, short-packet communications, satellite-terrestrial systems, block error rate, imperfect successive interference cancellation, reliability analysis.**

I. INTRODUCTION

Satellite–terrestrial communication systems have attracted significant interest as future 6G networks begin to demand wider coverage, massive connectivity, and reliable links for devices scattered across remote or hard-to-reach regions [1]–[3]. Unlike traditional broadband satellite services that focus on large codewords and high throughput, many emerging applications are now dominated by short-packet transmission, where only a few hundred symbols are available to encode critical information. Examples include environmental monitoring sensors, safety-related signaling, UAV telemetry packets, and low-latency control messages for distributed IoT systems [4], [5]. These scenarios impose tight reliability and delay requirements, making it difficult to rely solely on classical Shannon-capacity results, which assume infinitely long blocklengths and often mask the performance degradation triggered by short packets [6]–[8]. As a result, finite-blocklength (FBL) analysis has become increasingly important for understanding the practical behavior of satellite links operating under strict latency constraints [9].

Another challenge that satellite systems must contend with is interference management. With the growth of spectrum sharing between terrestrial and non-terrestrial networks, serving multiple ground users simultaneously requires access schemes that can sustain reliability in the presence of strong co-channel interference. Non-orthogonal multiple access (NOMA) has been widely studied for this purpose, but its dependence on accurate successive interference cancellation (SIC) often leads to performance loss when SIC becomes imperfect—something that occurs frequently in Shadowed-Rician fading, user mobility, or channel estimation uncertainty [10]–[13]. Even small SIC errors may propagate and severely deteriorate reliability, particularly when packets are short and decoding margins are tight [14], [15]. In contrast, rate-splitting multiple access (RSMA) has emerged as a more flexible strategy that can blend partial interference decoding with partial interference treating-as-noise [16]. By dividing messages into a common stream and several private streams, RSMA can distribute interference more evenly across users and reduce the system's sensitivity to imperfect SIC. Several recent studies have shown that RSMA tends to provide more stable throughput and outage performance than NOMA in satellite or integrated satellite–terrestrial networks [17], especially when channel conditions fluctuate or users have highly unbalanced link qualities. However, most of these studies evaluate RSMA under the infinite blocklength assumption, where error probabilities naturally vanish at high SNR and decoding imperfections are less visible. This leaves an important open question unanswered: How does RSMA behave in short-packet satellite links where reliability, not capacity, becomes the primary metric?

But another layer of complexity arises from the Shadowed-Rician fading environment that characterizes many land-mobile satellite links. Driven by the degree of shadowing-from average to heavy-deep signal fluctuations make the block error rate swing wildly, even when the average signal-to-noise ratio is the same. These swings are even tougher to manage under FBL constraints, where tight margins around the coding gain come into play. Understanding the interplay of RSMA, FBL limits, imperfect SIC, and Shadowed-Rician fading is critical to shaping robust next-generation satellite-terrestrial systems. In this spirit, the present paper provides a detailed framework for the study of RSMA-enabled satellite short-packet communication under FBL constraints. The scaling of

[(1)] Sang-Quang Nguyen is with Posts and Telecommunications Institute of Technology, Ho Chi Minh City 70000, Vietnam. (e-mail: sangnq@ptit.edu.vn)
[(2)] Chi-Bao Le is with Transcosmos Vietnam, Ho Chi Minh City, Vietnam. (e-mail: bao.lc@trans-cosmos.com.vn)
[(*)] Corresponding author.

DOI: 10.36244/ICJ.2026.1.8

reliability with transmit power, codeword length, shadowing severity, and power-splitting choices is derived, as well as a comparison of RSMA against NOMA to uncover practical differences in robustness. These contributions shall serve as guidelines for the system designer to identify regimes where RSMA yields actual gains and where its common-message approach stabilizes error performance in realistic satellite environments. Different from existing RSMA finite-blocklength studies that primarily consider terrestrial or uplink systems, and RSMA-based satellite works that typically assume infinite blocklength, this paper focuses on downlink low Earth orbit (LEO) satellite communications under finite-blocklength constraints, Shadowed-Rician fading, and imperfect SIC.

A. Motivations and Contributions

The main contributions of this paper are outlined as follows:

- We develop a finite-blocklength reliability framework for downlink RSMA-enabled LEO satellite systems over Shadowed-Rician channels, which captures the decoding behavior of both common and private messages under short-packet constraints while explicitly accounting for imperfect SIC, a combination that has not been jointly investigated in existing works.
- Closed-form approximations for the BLER of RSMA streams are derived, explicitly incorporating the impact of imperfect SIC (ipSIC), which is a realistic challenge for practical receivers in satellite environments.
- A detailed comparison with NOMA is presented, showing when and why RSMA provides more reliable short-packet transmission-particularly at moderate SNRs, under severe shadowing, or when the blocklength becomes tight.
- Extensive numerical results validate the analysis and illustrate how transmit power, antenna configuration, blocklength, and shadowing severity jointly shape the reliability of RSMA-based satellite links.

Compared to existing RSMA studies under the finite-blocklength regime, which mainly focus on terrestrial or uplink scenarios, this work investigates downlink RSMA transmission in LEO satellite systems over Shadowed-Rician channels. Moreover, unlike prior satellite RSMA analyses that typically rely on infinite blocklength assumptions, we explicitly characterize finite-blocklength BLER performance while accounting for imperfect SIC effects on both common and private streams.

B. Organization & Notations

The remainder of this paper is structured as follows. Section II describes the system model, including the satellite-terrestrial channel characteristics and the RSMA transmission strategy. Section III develops the finite-blocklength analysis and derives the corresponding expressions for the achievable performance. Section IV reports and discusses the numerical results, highlighting the comparison between RSMA and conventional multiple-access schemes. Finally, Section V summarizes the main findings and outlines potential directions for future work.

Notations: Throughout this paper, we use several frequently used mathematical symbols. The operator $\mathbb{E}\{.\}$ denotes expectation; $J_i(\cdot)$ refers to the Bessel function of the first kind with order i; $\|.\|_F$ is the Frobenius norm; ${}_1F_1(\cdot;\cdot;\cdot)$ represents the confluent hypergeometric function of the first kind; $(\cdot)_t$ is the Pochhammer symbol; $\mathcal{B}(\cdot,\cdot)$ corresponds to the Beta function; $\Gamma(\cdot)$ is the Gamma function; $\gamma(\cdot,\cdot)$ indicates the lower incomplete Gamma function; the Gaussian $\mathcal{Q}$-function is written as $\mathcal{Q}(x) = \frac{1}{2\pi}\int_x^\infty e^{-t^2/2}\,dt$; and for any random variable X, its probability density and cumulative distribution functions are denoted by $f_X(\cdot)$ and $F_X(\cdot)$, respectively.

II. System Model and Terrestrial Channel Model

A. System Description

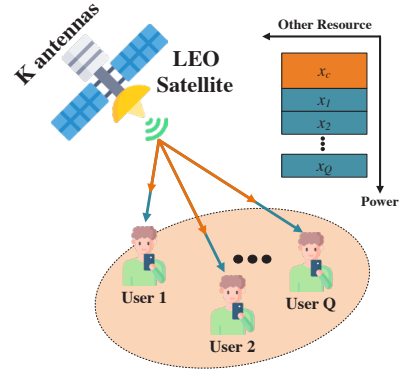

Fig. 1. An illustration of a downlink RSMA-enabled satellite-terrestrial communication system.

Fig. 1 sketches the downlink satellite-terrestrial network considered in this work, where rate-splitting multiple access (RSMA) is adopted. In this setup, a satellite S equipped with K antennas communicates simultaneously with Q ground users. The satellite operates in half-duplex mode and employs RSMA to handle interference while still aiming for better spectral efficiency. In practice, modern satellite platforms usually rely on multibeam architectures to extend coverage and capacity. For LEO systems, these beams are commonly produced by array-fed reflectors-mainly because they tend to be more efficient than direct radiating arrays. Since the beam pattern is fixed, the satellite avoids the need for heavy onboard signal processing.

The signal received at each user is shaped by the beamforming strategy, propagation environment, and power allocation used at the satellite. The channel gain from the satellite to user q is modeled as

$$\mathbf{h}_{U_q} = \mathcal{A}_q \mathbf{g}_{U_q}^{\dagger} \mathbf{w}_{U_q}, \tag{1}$$

where $\mathcal{A}_q$ includes both the antenna gain and free-space path-loss. The vector $\mathbf{g}_{U_q}$ represents the $K \times 1$ Shadowed-Rician fading channel between the satellite antennas and user q. The operator $(.)^{\dagger}$ denotes the conjugate transpose, and $\mathbf{w}_{U_q}$ is the corresponding $K \times 1$ beamforming vector. Following the maximum ratio transmission (MRT) rule, the beamformer is

selected as $\mathbf{w}_{U_q} = \frac{\|\mathbf{g}_{U_q}\|}{\|\mathbf{g}_{U_q}\|_F}$, where $\|.\|_F$ is the Frobenius norm. The factor $\mathcal{A}_q$ remains fixed and is written as

$$\mathcal{A}_q = \frac{c\sqrt{G_S G_R}}{4\pi f_c d_{S_q}}, \tag{2}$$

Here, c and f_c denoting the speed of light and the carrier frequency. The term d_{S_q} is the distance between the satellite and user q. The gains G_S and G_R correspond to the satellite beam gain and the user terminal gain, respectively. Specifically, $G_S = G_{\max}\left[\frac{J_1(w)}{2w} + 36\frac{J_3(w)}{w^3}\right]^2$, where $G_{\max}$ is the maximum beam gain and $w = \frac{2.07123\sin(\theta)}{\sin(\theta_{3\text{dB}})}$. Here, θ denotes the angular offset from the beam center, $\theta_{3\text{dB}}$ the 3 dB beamwidth, and $J_1(\cdot)$, $J_3(\cdot)$ are Bessel functions of order 1 and 3. In this model, different users are separated based on their channel quality obtained, for example, via pilot-assisted channel estimation. We further assume ideal CSI at the transmitter, and the results serve as a reference for future studies involving CSI imperfections [18].

B. The signal processing at transceivers

The satellite employs RSMA to serve all users concurrently. The transmitted waveform consists of two parts: a common message, intended to be decoded by every user, and a private message for each individual user. A power coefficient a_c is assigned to the common stream, whereas the remaining power is split among the private streams.

The transmitted signal is expressed as

$$x = \sqrt{P_S}\left(\sqrt{a_c}x_c + \sum\nolimits_{q=1}^{Q}\sqrt{a_q}x_q\right), \tag{3}$$

where P_S is the satellite transmit power, x_c is the common message with power $a_c P_S$, and x_q is the private message for user q with power $a_q P_S$. It holds that $a_c + \sum_{q=1}^{Q} a_q = 1$. The received signal at user q is then

$$\begin{aligned} y_{U_q} =& \mathbf{h}_{U_q}x + n_{U_q} \\ =& \underbrace{\mathbf{g}_{U_q}^{\dagger}\mathbf{w}_{U_q}\mathcal{A}_q\sqrt{a_c P_S}x_c}_{\text{Common Message}} + \underbrace{\mathbf{g}_{U_q}^{\dagger}\mathbf{w}_{U_q}\mathcal{A}_q\sqrt{a_q P_S}x_q}_{\text{Private Message}} \\ &+ \underbrace{\sum\nolimits_{j=1,j\neq q}^{Q}\mathbf{g}_{U_q}^{\dagger}\mathbf{w}_{U_q}\mathcal{A}_q\sqrt{a_j P_S}x_j}_{\text{Interference}} + \underbrace{n_{U_q}}_{\text{AWGN}}, \end{aligned} \tag{4}$$

where n_{U_q} is AWGN with zero mean and variance N_0. Each user decodes the received signal in two steps.

C. Decoding the common message

Users start by decoding the common message x_c while considering the private streams as interference. The SINR for decoding the common message at user q is

$$\begin{aligned} \bar{\gamma}_{c,q} =& \frac{a_c\mathcal{A}_q^2 P_S\left\|\mathbf{g}_{U_q}\right\|_F^2}{N_0 + \mathcal{A}_q^2 P_S\left(1-a_c\right)\left\|\mathbf{g}_{U_q}\right\|_F^2} \\ =& \frac{a_c\mathcal{C}_q}{1+\left(1-a_c\right)\mathcal{C}_q}, \end{aligned} \tag{5}$$

where $\varrho_S = \frac{P_S}{N_0}$ is the signal-to-noise ratio (SNR), $\mathcal{C}_q = \delta_q\left\|\mathbf{g}_{U_q}\right\|_F^2$ and $\delta_q = \varrho_S\mathcal{A}_q^2$.

D. Decoding the private message

After removing the common message, user q proceeds to decode its own private message. Interference now comes only from private messages of other users. The SINR for private decoding is

$$\bar{\gamma}_{p,q} = \frac{a_q\mathcal{C}_q}{1+\mathcal{C}_q\sum_{j=1,q\neq j}^{Q}a_j + \Xi_q a_c\mathcal{C}_q}, \tag{6}$$

where Ξ_q accounts for imperfect SIC (ipSIC), with $\Xi_q = 0$ corresponding to ideal cancellation [19].

E. Terrestrial Channel Model

To analyze performance metrics later on, we assume the fading coefficients are i.i.d. The PDF of the channel coefficient $g_{U_q}^{(k)}$ from the kth satellite antenna to user q is

$$f_{\left|g_{U_q}^{(k)}\right|^2}(x) = \alpha_q e^{-\beta_q x}{}_1F_1\left(m_q;1;\varpi_q x\right)\ ,\ x\geq 0\ , \tag{7}$$

where α_q, β_q, and ϖ_q are defined as in the original expression, with Ω_q, $2b_q$, and m_q denoting the LOS power, multipath power, and fading severity, respectively. The term ${}_1F_1(\cdot)$ is the confluent hypergeometric function [20, Eq. (9.210.1)].

Assuming m_q takes integer values, the PDF simplifies to

$$f_{\left|g_{U_q}^{(k)}\right|^2}(x) = \alpha_q e^{-(\beta_q-\varpi_q)x}\sum_{t=0}^{m_q-1}\zeta_q(t)\,x^t\ ,\ x\geq 0\ , \tag{8}$$

in which $\zeta_q(t)$ defined in terms of the Pochhammer symbol. Using [21], the PDF of $\mathcal{C}_q$ under i.i.d. Shadowed-Rician fading is

$$f_{\mathcal{C}_q}(x) = \sum_{j_1=0}^{m_q-1}\cdots\sum_{j_K=0}^{m_q-1}\frac{\Lambda_q(K)}{\delta_q^{\Delta_q}}x^{\Delta_q-1}e^{-\left(\frac{\psi_q}{\delta_q}\right)x}, \tag{9}$$

where

$$\Lambda_q(K) = \alpha_q^K\prod\nolimits_{l=1}^{K}\zeta_q(j_l)\prod\nolimits_{u=1}^{K-1}\mathcal{B}\left(\sum\nolimits_{p=1}^{u}j_p+u, j_{u+1}+1\right), \tag{10}$$

and

$$\Delta_q = \sum\nolimits_{l=1}^{K}j_l + K,\quad \psi_q = \beta_q - \delta_q. \tag{11}$$

Applying [20, Eq. (3.351.1)], the CDF of $\mathcal{C}_q$ becomes

$$F_{\mathcal{C}_q}(x) = \sum_{j_1=0}^{m_q-1}\cdots\sum_{j_K=0}^{m_q-1}\frac{\Lambda_q(K)}{\psi_q^{\Delta_q}}\gamma\left(\Delta_q, \frac{\psi_q x}{\delta_q}\right), \tag{12}$$

which can be further simplified via [20, Eq. (8.352.6)] to

$$F_{\mathcal{C}_q}(x) = 1 - \sum_{j_1=0}^{m_q-1}\cdots\sum_{j_K=0}^{m_q-1}\sum_{p=0}^{\Delta_q-1}\frac{\Lambda_q(K)\,\Gamma(\Delta_q)}{p!\psi_q^{\Delta_q-p}\delta_q^p}e^{-\frac{\psi_q x}{\delta_q}}x^p. \tag{13}$$

Remark 1: This characterization highlights how the channel statistics influence system behavior under the Shadowed-Rician fading considered in this work.

III. FINITE-BLOCKLENGTH ANALYSIS

In this section, we analyze the reliability performance of the RSMA-enabled satellite-terrestrial system when short-packet transmission is adopted. Unlike the infinite blocklength (IBL) regime, where decoding errors can be made arbitrarily small, finite-blocklength (FBL) theory reveals that the block error rate (BLER) remains strictly positive even when the coding rate lies below Shannon capacity. Therefore, the performance of the satellite link must be re-evaluated under the FBL regime to support delay-critical satellite applications such as emergency response, low-latency sensing, and real-time IoT services.

Throughout this section, the SINRs used for decoding the common and private RSMA messages follow (5) and (6), and the distribution of the effective channel gain $\mathcal{A}_q$ follows the Shadowed-Rician model in (9)-(13) in Section II.

A. Reliability Analysis

The decoding reliability at user U_q for both the common message and the private message can be approximated using the finite-blocklength framework. For moderately large blocklengths (typically $\mathcal{L}_{a,q} > 100$), the instantaneous BLER can be written as

$$\varepsilon_{a,q} \simeq \mathcal{Q}\left(\frac{\mathcal{C}(\bar{\gamma}_{a,q}) - \mathcal{R}_{a,q}}{\sqrt{\mathcal{V}(\bar{\gamma}_{a,q})\,\mathcal{L}_{a,q}^{-1}}}\right), \qquad a \in \{c, p\}, \tag{14}$$

where $a = c$ corresponds to the common message and $a = p$ refers to the private message. Here, $\mathcal{R}_{a,q} = \mathcal{T}_{a,q}/\mathcal{L}_{a,q}$ denotes the coding rate, with $\mathcal{L}_{a,q}$ being the blocklength and $\mathcal{T}_{a,q}$ the number of transmitted information bits. The term $\mathcal{C}(\bar{\gamma}_{a,q}) = \log_2(1+\bar{\gamma}_{a,q})$ represents the Shannon capacity associated with the received SINR $\bar{\gamma}_{a,q}$, while the channel dispersion is given by $\mathcal{V}(\bar{\gamma}_{a,q}) = \left[1 - (1+\bar{\gamma}_{a,q})^{-2}\right](\log_2 e)^2$. The function $\mathcal{Q}(\cdot)$ stands for the Gaussian Q-function.

From (14), the average BLER at user U_q for decoding both the common message and the private message can be expressed as

$$\tilde{\varepsilon}_{a,q} = \mathbb{E}\left\{\varepsilon_{a,q}\right\}. \tag{15}$$

The total average BLER at user U_q, denoted by $\tilde{\varepsilon}_q$, is obtained by averaging the BLER contributions from both the common and private messages. Accordingly, based on (15), we can write

$$\tilde{\varepsilon}_q = (\tilde{\varepsilon}_{c,q} + \tilde{\varepsilon}_{p,q})/2. \tag{16}$$

The closed-form formulation of the average BLER at each user is obtained in the following proposition.

Proposition 1: The closed-form approximate expression for the total average BLER at user U_q, denoted by $\tilde{\varepsilon}_q$, can be written as

$$\begin{aligned}\tilde{\varepsilon}_q \approx \frac{1}{2}\Bigg\langle &\Bigg[1 - \sum_{t=1}^{\mathbb{T}} \frac{1}{\mathbb{T}} \sum_{j_1=0}^{m_q-1} \cdots \sum_{j_K=0}^{m_q-1} \sum_{p=0}^{\Delta_q-1} \frac{\Lambda_q(K)\,\Gamma(\Delta_q)}{p!\psi_q^{\Delta_q-p}\delta_q^p} \\ &\times e^{-\frac{\psi_q}{\delta_q}\left(\frac{\Phi_{c,q}}{a_c - \Phi_{c,q}(1-a_c)}\right)} \left(\frac{\Phi_{c,q}}{a_c - \Phi_{c,q}(1-a_c)}\right)^p\Bigg] \\ &+ \Bigg[1 - \sum_{t=1}^{\mathbb{T}} \frac{1}{\mathbb{T}} \sum_{j_1=0}^{m_q-1} \cdots \sum_{j_K=0}^{m_q-1} \sum_{p=0}^{\Delta_q-1} \frac{\Lambda_q(K)\,\Gamma(\Delta_q)}{p!\psi_q^{\Delta_q-p}\delta_q^p} \\ &\times e^{-\frac{\psi_q}{\delta_q}\left(\frac{\Phi_{p,q}}{a_q - \Phi_{p,q}\left(\sum_{j=1,q\neq j}^{Q} a_j + \Xi_q a_c\right)}\right)} \\ &\times \left(\frac{\Phi_{p,q}}{a_q - \Phi_{p,q}\left(\sum_{j=1,q\neq j}^{Q} a_j + \Xi_q a_c\right)}\right)^p\Bigg]\Bigg\rangle.\end{aligned} \tag{17}$$

Remark 2: Under imperfect SIC, the average BLER does not vanish at high SNR and instead converges to an error floor dominated by residual interference. The impact of finite blocklength enters through the channel dispersion term, which becomes more pronounced in the short-packet regime. In this setting, RSMA benefits from the common stream, which provides an additional decoding layer and reduces sensitivity to residual interference compared to NOMA. Consequently, RSMA exhibits more stable reliability, particularly at moderate SNRs where finite-blocklength effects and imperfect SIC jointly limit performance.

Proof: Substituting $\varepsilon_{a,q}$ from (14) to (15), the average BLER at U_q for decoding both the common message and the private message can be expressed as

$$\tilde{\varepsilon}_{a,q} \simeq \mathbb{E}\left\{\mathcal{Q}\left(\frac{\mathcal{C}(\bar{\gamma}_{a,q}) - \mathcal{R}_{a,q}}{\sqrt{\mathcal{V}(\bar{\gamma}_{a,q})\,\mathcal{L}_{a,q}^{-1}}}\right)\right\}. \tag{18}$$

Obtaining a closed-form expression for (18) is, unfortunately, analytically intractable. For this reason, and following the approach in [22], we approximate $\tilde{\varepsilon}_{a,q}$ by

$$\tilde{\varepsilon}_{a,q} \approx \int_0^\infty \Upsilon_{a,q}(x)\, f_{\bar{\gamma}_{a,q}}(x)\, dx, \tag{19}$$

where $f_{\bar{\gamma}_{a,q}}(\cdot)$ denotes the PDF of the received SINR $\bar{\gamma}_{a,q}$. The function $\Upsilon_{a,q}(\cdot)$ serves as a tractable approximation of the term $\mathcal{Q}\left(\frac{\mathcal{C}(\bar{\gamma}_{a,q}) - \mathcal{R}_{a,q}}{\sqrt{\mathcal{V}(\bar{\gamma}_{a,q})\,\mathcal{L}_{a,q}^{-1}}}\right)$ and might be expressed as

$$\Upsilon_{a,q}(\bar{\gamma}_{a,q}) = \begin{cases} 1, & \bar{\gamma}_{a,q} \le \phi_{a,q}, \\ 0.5 - \mathcal{G}_{a,q}\sqrt{\mathcal{L}_{a,q}}\,(\bar{\gamma}_{a,q} - \chi_{a,q}), & \phi_{a,q} < \bar{\gamma}_{a,q} < \varsigma_{a,q}, \\ 0, & \bar{\gamma}_{a,q} \ge \varsigma_{a,q}, \end{cases} \tag{20}$$

where $\mathcal{G}_{a,q} = \left(2\pi\sqrt{2^{2\mathcal{R}_{a,q}} - 1}\right)^{-1}$, $\chi_{a,q} = 2^{\mathcal{R}_{a,q}} - 1$, $\phi_{a,q} = \chi_{a,q} - \left(2\mathcal{G}_{a,q}\sqrt{\mathcal{L}_{a,q}}\right)^{-1}$, and $\varsigma_{a,q} = \chi_{a,q} + \left(2\mathcal{G}_{a,q}\sqrt{\mathcal{L}_{a,q}}\right)^{-1}$. Next, by following the approach in [19] and applying integration by parts, the expression in (19) can be simplified as

$$\tilde{\varepsilon}_{a,q} \approx \mathcal{G}_{a,q}\sqrt{\mathcal{L}_{a,q}} \int_{\phi_{a,q}}^{\varsigma_{a,q}} F_{\bar{\gamma}_{a,q}}(x) dx. \tag{21}$$

Since the gap between $\phi_{a,q}$ and $\varsigma_{a,q}$ in (19) is relatively small [23], $\tilde{\varepsilon}_{a,q}$ can be further simplified by

$$\tilde{\varepsilon}_{a,q} \approx \begin{cases} \sum_{t=1}^{\mathbb{T}} \frac{1}{\mathbb{T}} F_{\mathcal{C}_q}\left(\frac{\Phi_{a,q}}{a_c - \Phi_{a,q}(1-a_c)}\right), & a \in c, \\ \sum_{t=1}^{\mathbb{T}} \frac{1}{\mathbb{T}} F_{\mathcal{C}_q}\left(\frac{\Phi_{a,q}}{a_q - \Phi_{a,q}\left(\sum_{j=1, q\neq j}^{Q} a_j + \Xi_q a_c\right)}\right), & a \in p, \end{cases} \tag{22}$$

Here, $\mathbb{T}$ implies the complexity accuracy trade-off parameter and $\Phi_{a,q} = \phi_{a,q} + (2t-1)(\varsigma_{a,q} - \phi_{a,q})/2\mathbb{T}$.

Using (13) and (22), we can derive the close-form of $\tilde{\varepsilon}_{a,q}$ as

$$\tilde{\varepsilon}_{a,q} \approx 1 - \sum_{t=1}^{\mathbb{T}} \frac{1}{\mathbb{T}} \sum_{j_1=0}^{m_q-1} \cdots \sum_{j_K=0}^{m_q-1} \sum_{p=0}^{\Delta_q-1} \frac{\Lambda_q(K)\,\Gamma(\Delta_q)}{p!\psi_q^{\Delta_q-p}\delta_q^p} \times e^{-\frac{\psi_q \xi_{a,q}}{\delta_q}} \xi_{a,q}^p, \tag{23}$$

where $\xi_{a,q} = \frac{\Phi_{a,q}}{a_c - \Phi_{a,q}(1-a_c)}$ for the common part ($a = c$), whereas for the private part ($a = p$), it is given by $\xi_{a,q} = \frac{\Phi_{a,q}}{a_q - \Phi_{a,q}\left(\sum_{j=1, j\neq q}^{Q} a_j + \Xi_q\right) a_c}$.

We derive the closed-form expression of the average BLER at each user in (17) by substituting (23) in (16).

The proof is completed. ■

Reliability at U_q is the chance that the packet is accurately identified, given as [24, Eq. (27)]

$$\nu_q = (1 - \tilde{\varepsilon}_q) \times 100\%. \tag{24}$$

Furthermore, the throughput for each user may be assessed as

$$\tau_q = (1 - \tilde{\varepsilon}_{c,q})\,\mathcal{R}_{c,q} + (1 - \tilde{\varepsilon}_{p,q})\,\mathcal{R}_{p,q}. \tag{25}$$

IV. Results and Discussions

In this segment, we conduct a series of numerical simulations to check how well the analytical expressions capture the behavior of the considered RSMA-enabled satellite-terrestrial system. The Shadowed-Rician fading parameters are chosen according to two typical shadowing conditions often used in satellite literature [25]: an average-shadowing case with $(b_q, m_q, \Omega_q) = (0.251, 5, 0.279)$ and a heavier shadowing scenario characterized by $(0.063, 1, 0.0007)$. To keep the setup simple, the system involves two terrestrial users ($Q = 2$), $\mathcal{L} = \mathcal{L}_{c,q} = \mathcal{L}_{p,q} = 200$, $\mathcal{T} = \mathcal{T}_{c,q} = \mathcal{T}_{p,q} = 80$ bits, both assumed to experience the same SIC imperfection level, i.e., $\Xi = \Xi_1 = \Xi_2$ and $\mathbb{T} = 5$. The equivalent noise power at each user terminal is modeled as $N_0 = \kappa B_w T$, where $\kappa = 1.38 \times 10^{-23}$ denotes the Boltzmann constant, $B_w = 50$ MHz is the transmission bandwidth, and the noise temperature is set to $T = 290$ K, a value commonly used for LEO downlink links [26]. The satellite operates with $K = 2$ antennas and radiates from a LEO platform toward a ground terminal located about $d_{S_q} = 1000$ km away. The carrier frequency is $f_c = 1.55$ GHz, and the propagation constants follow the typical free–space path-loss model. For the antenna characteristics, we adopt a receive antenna gain of $G_R = 5$ dBi and a maximum satellite beam gain of $G_{\max} = 25$ dBi, with an angular separation of $\theta = 0.8°$ between the users and a 3-dB beamwidth of $\theta_{3\text{dB}} = 0.4°$. To evaluate the system performance under these settings, each simulation curve is averaged over 10^6 Monte Carlo realizations. Regarding the power distribution, the common-message power ratio is fixed at $a_c = 0.4$, and the remaining power is proportionally divided among the users according to $a_1 = 0.4(1 - a_c)$ and $a_2 = 0.6(1 - a_c)$, reflecting a mild imbalance in private-message allocation. For NOMA, a fixed power allocation and the conventional SIC decoding order are assumed, which are commonly adopted for baseline comparisons.

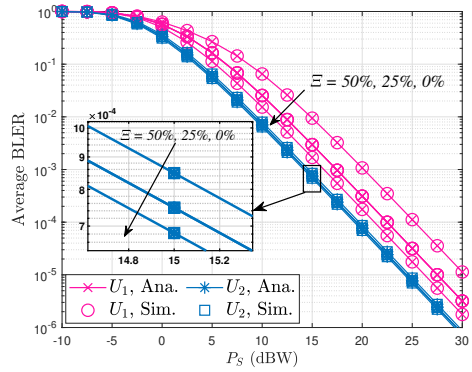

Fig. 2. Average BLER versus transmit power for different levels of SIC imperfection, with $K = 2$.

In Figure 2, we examine how the average BLER varies with transmit power under different levels of SIC imperfection. As expected, all curves improve gradually as the SNR increases, but the presence of residual interference still leaves a visible gap between the ideal and imperfect cases. At low SNR, the average BLER of all curves remains relatively high and close together, suggesting that noise dominates in this region. When the SNR approaches the medium range, the impact of the errors in the SIC starts becoming significant, and a small level of imprecision causes the average BLER convergence speed to reduce. For the high SNR range, it appears that the system with the highest level of imprecision for the SIC will eventually converge to the error floor, which suggests that the presence of the interference will affect the reliability of the RSMA, even when it operates at higher powers.

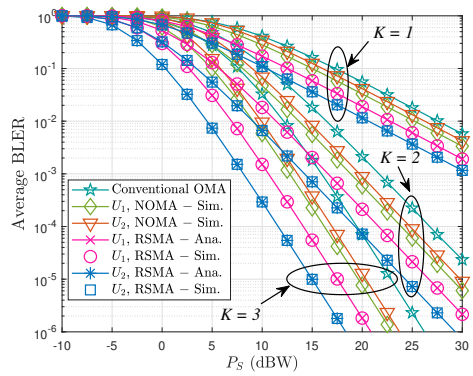

Fig. 3. Average BLER versus transmit power with increasing number of antennas at the satellite, for $\Xi = 10\%$.

Figure 3 illustrates the impact of the number of satellite antennas on the BLER performance of RSMA, NOMA, and conventional OMA. As the antenna number increases, RSMA tends to achieve a more pronounced BLER reduction, benefiting more effectively from the additional array gain. In the low-SNR region, the performance of RSMA and NOMA remains close, since noise largely dominates the system behavior. Once the SNR exceeds a certain threshold, however, a clear performance separation emerges, with RSMA outperforming both NOMA and OMA. It is also apparent that $K = 3$, the RSMA curve drops more rapidly than those of NOMA and conventional OMA, which highlights the effectiveness of multi-antenna processing combined with rate-splitting. At higher SNR values, this performance advantage is largely preserved, while the improvement of NOMA gradually saturates due to residual interference.

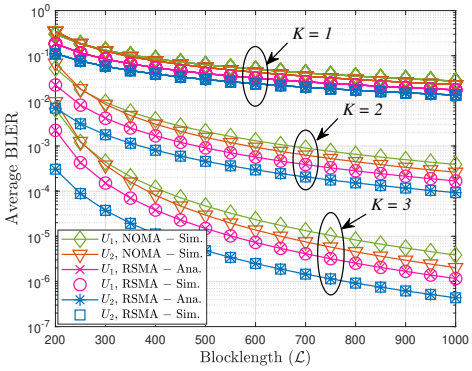

Fig. 4. Average BLER versus blocklength with increasing number of antennas at the satellite, for $\Xi = 20\%$ and $P_S = 10$ dBW.

Figure 4 examines the impact of blocklength on the BLER performance of RSMA and NOMA. As expected, increasing the blocklength improves reliability for both schemes due to reduced channel dispersion. However, RSMA exhibits a faster BLER decay, particularly in the short and moderate blocklength regimes, since the common message provides an additional decoding path for users experiencing unfavorable channel conditions. In contrast, NOMA degrades more rapidly when packets are short, as its performance relies heavily on reliable SIC, which becomes less effective under FBL. As the blocklength grows large, the performance gap gradually narrows and eventually saturates, indicating diminishing FBL effects. Overall, the results suggest that RSMA achieves higher reliability and better energy efficiency than NOMA in short-packet satellite transmissions.

Figure 5 illustrates the BLER behavior of the satellite link under average shadowing (AS) and heavy shadowing (HS) conditions. Under AS, where signal blockage is moderate, the channel remains relatively stable and BLER decreases rapidly with increasing transmit power. In contrast, HS introduces severe signal obstruction and deep fading, resulting in persistently higher BLER and a much slower improvement even with power boosting. These results indicate that while RSMA remains robust under AS conditions, severe shadowing imposes a fundamental limitation that cannot be fully mitigated by transmit power alone.

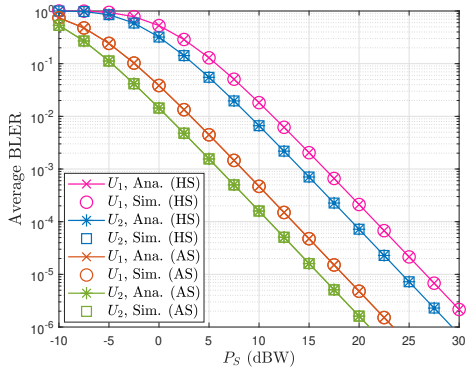

Fig. 5. Average BLER versus transmit power under various shadow fading, with $\Xi = 10\%$ and $K = 2$.

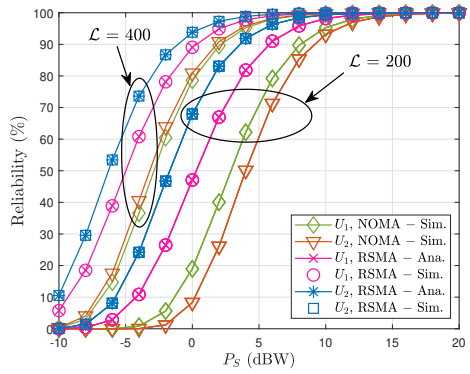

Fig. 6. Reliability versus transmit power for different blocklength values, with $\Xi = 10\%$ and $K = 2$.

Figure 6 presents the reliability performance versus transmit power for different blocklengths, comparing RSMA and NOMA. For all blocklength values, increasing power enhances reliability; however, RSMA consistently achieves a target BLER at lower SNR than NOMA. This advantage becomes more pronounced for short packets, where NOMA suffers from residual interference and imperfect SIC, leading to a noticeably higher BLER in the mid-SNR region. As the blocklength increases, both schemes benefit, yet RSMA maintains a clear edge owing to its common stream, which provides additional decoding robustness. These observations confirm that RSMA is more suitable for reliability-critical short-packet satellite links.

Finally, Figure 7 compares the throughput performance of RSMA and NOMA under different satellite antenna configurations. Increasing the transmit power improves throughput for both schemes; however, RSMA consistently achieves higher throughput due to its superior decoding reliability. Moreover, the use of additional antennas enhances the SINR of both common and private streams in RSMA, allowing it to better exploit spatial diversity. At moderate SNR, RSMA exhibits a steeper throughput increase, whereas NOMA remains constrained by

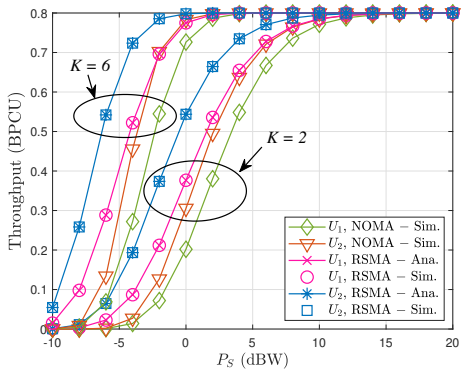

Fig. 7. Throughput versus transmit power with increasing number of antennas at the satellite, for $\Xi = 10\%$ and $K = \{2, 6\}$.

residual interference and BLER effects. Even at high SNR, the throughput gap persists, highlighting that RSMA more effectively converts reliability gains into throughput benefits under short-packet conditions.

It is worth noting that the analytical and simulation results presented in this section are obtained under the assumption of perfect CSI at the receiver. In practical LEO satellite systems, channel estimation errors may arise due to mobility, Doppler effects, and limited pilot resources, which can degrade the reliability performance to some extent. Nevertheless, the results reported here serve as a useful benchmark for evaluating the fundamental behavior of RSMA under finite-blocklength transmission. Incorporating CSI imperfections into the proposed framework is an interesting extension and will be considered in future work.

V. CONCLUSION

This paper explored how RSMA behaves in satellite short-packet communications when finite-blocklength and realistic channel conditions are taken into account. By building a tractable FBL model over Shadowed-Rician fading, we derived BLER expressions for both common and private streams, including the effect of imperfect SIC–something that often becomes a real bottleneck in practical receivers. The analysis and simulations align well and point to a consistent trend: RSMA tends to hold its reliability better than NOMA, especially when the packets are short or the shadowing becomes heavy. The common stream, although simple in structure, seems to play a meaningful role in stabilizing the error performance when the SNR is moderate and when ipSIC degrades the private layers. Numerical results further show that RSMA normally requires less transmit power to reach comparable BLER targets and scales more gracefully with blocklength and antenna count. While this study focused on a basic two-user setting, the insights suggest that RSMA is a promising direction for future satellite systems that must deliver reliable, low-latency short-packet links. Extending the model to multi-beam satellites, multi-user scenarios, or imperfect CSI would be a natural next step for future work.

REFERENCES

[1] X. Liu, K.-Y. Lam, F. Li, J. Zhao, L. Wang, and T. S. Durrani, "Spectrum sharing for 6g integrated satellite-terrestrial communication networks based on noma and cr," *IEEE Network*, vol. 35, no. 4, pp. 28–34, 2021. DOI: 10.1109/MNET.011.2100021.

[2] X. Fang, W. Feng, T. Wei, Y. Chen, N. Ge, and C.-X. Wang, "5g embraces satellites for 6g ubiquitous iot: Basic models for integrated satellite terrestrial networks," *IEEE Internet of Things Journal*, vol. 8, no. 18, pp. 14 399–14 417, 2021. DOI: 10.1109/JIOT.2021.3068596.

[3] Q. Wang, X. Chen, and Q. Qi, "Energy-efficient design of satellite-terrestrial computing in 6g wireless networks," *IEEE Transactions on Communications*, vol. 72, no. 3, pp. 1759–1772, 2024. DOI: 10.1109/TCOMM.2023.3334813.

[4] N. Abbas, A. Mrad, A. Ghazleh, and S. Sharafeddine, "Uav-based relay system for iot networks with strict reliability and latency requirements," *IEEE Networking Letters*, vol. 3, no. 3, pp. 110–113, 2021. DOI: 10.1109/LNET.2021.3077869.

[5] E. E. Haber, H. A. Alameddine, C. Assi, and S. Sharafeddine, "Uav-aided ultra-reliable low-latency computation offloading in future iot networks," *IEEE Transactions on Communications*, vol. 69, no. 10, pp. 6838–6851, 2021. DOI: 10.1109/TCOMM.2021.3096559.

[6] C. Feng, H.-M. Wang, and H. V. Poor, "Reliable and secure short-packet communications," *IEEE Transactions on Wireless Communications*, vol. 21, no. 3, pp. 1913–1926, 2022. DOI: 10.1109/TWC.2021.3108042.

[7] J. Cao, X. Zhu, S. Sun, Z. Wei, Y. Jiang, J. Wang, and V. K. Lau, "Toward industrial metaverse: Age of information, latency and reliability of short-packet transmission in 6g," *IEEE Wireless Communications*, vol. 30, no. 2, pp. 40–47, 2023. DOI: 10.1109/MWC.2001.2200396.

[8] X. Gao, L. Shi, Y. Ye, G. Zheng, and G. Lu, "Reliability-oriented resource allocation in short-packet backscatter communications," *IEEE Transactions on Vehicular Technology*, vol. 74, no. 2, pp. 3468–3473, 2025. DOI: 10.1109/TVT.2024.3472093.

[9] J. Xu, O. Dizdar, and B. Clerckx, "Rate-splitting multiple access for short-packet uplink communications: A finite blocklength analysis," *IEEE Communications Letters*, vol. 27, no. 2, pp. 517–521, 2023. DOI: 10.1109/LCOMM.2022.3226817.

[10] H. Shuai, K. Guo, K. An, Y. Huang, and S. Zhu, "Transmit antenna selection in noma-based integrated satellite-hap-terrestrial networks with imperfect csi and sic," *IEEE Wireless Communications Letters*, vol. 11, no. 8, pp. 1565–1569, 2022. DOI: 10.1109/LWC.2022.3165710.

[11] G. Xu, Z. Zhao, Z. Song, Q. Zhang, and B. Ai, "Symbol error analysis for integrated satellite- terrestrial relay networks with non-orthogonal multiple access under hardware impairments," *IEEE Transactions on Wireless Communications*, vol. 23, no. 10, pp. 12 980–12 994, 2024. DOI: 10.1109/TWC.2024.3397847.

[12] S. Mondal, K. Singh, D. W. Kwan Ng, C.-P. Li, and Z. Ding, "Outage performance of ris-aided noma isac network for leo satellite system," in *2025 IEEE International Conference on Communications Workshops (ICC Workshops)*, 2025, pp. 1556–1561. DOI: 10.1109/ICCWorkshops67674.2025.11162359.

[13] Z. Belső and L. Pap, "Effect of the imperfect channel estimation on achievable noma rate," vol. 17, no. 1, pp. 2–10, 2023. DOI: 10.21203/rs.3.rs-3310816/v1.

[14] H. Zeng, R. Zhang, X. Zhu, J. Cao, Y. Jiang, F.-C. Zheng, and P. Dai, "Frame structure and resource optimization for hybrid long- and short-packet noma-based data collection in iiot with imperfect sic," *IEEE Internet of Things Journal*, vol. 11, no. 23, pp. 37 799–37 812, 2024. DOI: 10.1109/JIOT.2024.3444462.

[15] S. Kumar, B. Kumbhani, and S. Darshi, "Performance analysis of star-ris aided short-packet noma network under imperfect sic and csi," *IEEE Systems Journal*, vol. 19, no. 2, pp. 600–611, 2025. DOI: 10.1109/JSYST.2025.3562732.

[16] V. S. Nguyen, A. Le-Thi, V. D. Thuan, C.-B. Le, T. H. Nguyen, and S.-Q. Nguyen, "Analysis of ergodic sum rate in rsma with perfect and imperfect sic: A multiple-antenna selection approach for optimizing uav positioning," *Physical Communication*, vol. 72, p. 102 741, 2025. DOI: 10.1016/j.phycom.2025.102741.

[17] C. Hu, H. Yang, Z. Zhou, B. Li, X. Jiang, N. Zhao, and A. Nal- lanathan, "Outage analysis of rsma enabled integrated satellite-terrestrial networks," *IEEE Transactions on Vehicular Technology*, vol. 74, no. 6, pp. 10 023–10 028, 2025. DOI: 10.1109/TVT.2025.3539758.

[18] C. K. Singh, P. K. Upadhyay, J. Lehtomäki, and M. Juntti, "Performance analysis with deep learning assay for cooperative uav-borne irs noma networks under non-ideal system imperfections," *IEEE Transactions on Vehicular Technology*, vol. 73, no. 1, pp. 1065–1083, 2024. DOI: 10.1109/TVT.2023.3309619.

[19] S. K. Singh, K. Agrawal, K. Singh, Y.-M. Chen, and C.-P. Li, "Performance analysis and optimization of rsma enabled uav-aided ibl and fbl communication with imperfect sic and csi," *IEEE Transactions on Wireless Communications*, vol. 22, no. 6, pp. 3714–3732, 2023. DOI: 10.1109/TWC.2022.3220785.

[20] I. S. Gradshteyn and I. M. Ryzhik, Table of integrals, series, and products. *Academic press*, 2014. DOI: 10.1016/C2010-0-648395.

[21] V. Bankey, P. K. Upadhyay, D. B. Da Costa, P. S. Bithas, A. G. Kanatas, and U. S. Dias, "Performance analysis of multi-antenna multiuser hybrid satellite-terrestrial relay systems for mobile services delivery," *IEEE Access*, vol. 6, pp. 24 729–24 745, 2018. DOI: 10.1109/ACCESS.2018.2830801.

[22] C. D. Ho, T.-V. Nguyen, T. Huynh-The, T.-T. Nguyen, D. B. da Costa, and B. An, "Short-packet communications in wireless-powered cognitive iot networks: Performance analysis and deep learning evaluation," *IEEE Transactions on Vehicular Technology*, vol. 70, no. 3, pp. 2894–2899, 2021. DOI: 10.1109/TVT.2021.3061157.

[23] T.-H. Vu, T.-V. Nguyen, Q.-V. Pham, D. Benevides da Costa, and S. Kim, "Star-ris-enabled short-packet noma systems," *IEEE Transactions on Vehicular Technology*, vol. 72, no. 10, pp. 13 764–13 769, 2023. DOI: 10.1109/TVT.2023.3278737.

[24] G. N. Tran and S. Kim, "Performance analysis of short packets in noma vlc systems," *IEEE Access*, vol. 10, pp. 6505–6517, 2022. DOI: 10.1109/ACCESS.2022.3141865.

[25] N. I. Miridakis, D. D. Vergados, and A. Michalas, "Dual-hop communication over a satellite relay and shadowed rician channels," *IEEE Transactions on Vehicular Technology*, vol. 64, no. 9, pp. 4031–4040, 2015. DOI: 10.1109/TVT.2014.2361832.

[26] A. Abdi, W. Lau, M.-S. Alouini, and M. Kaveh, "A new simple model for land mobile satellite channels: first- and second-order statistics," *IEEE Transactions on Wireless Communications*, vol. 2, no. 3, pp. 519–528, 2003. DOI: 10.1109/TWC.2003.811182.

Sang-Quang Nguyen received the B.E. degree in Electrical Engineering from Ho Chi Minh City University of Transport, Vietnam, in 2010, the M.E. degree in Telecommunications Engineering from Ho Chi Minh City University of Technology, Vietnam, in 2013, and the Ph.D. degree in Electrical Engineering from the University of Ulsan, South Korea, in 2017. From 2017 to 2021, he was a Lecturer at Duy Tan University, Vietnam. Since May 2021, he has been a Lecturer at Ho Chi Minh City University of Transport, Vietnam. In September 2024, he joined the Post and Telecommunications Institute of Technology, Ho Chi Minh City, as a Lecturer. He also served as a Research Fellow at Queen's University Belfast, United Kingdom, where he contributed to advancements in wireless communications. Dr. Sang's research interests include cooperative communications, cognitive radio networks, physical layer security, non-orthogonal multiple access (NOMA), short-packet communications, and backscatter communications. His work primarily focuses on secure and energy-efficient communication solutions for next-generation wireless networks. Dr. Sang can be contacted via email at sangnq@ptit.edu.vn.

Chi-Bao LE was born in Binh Thuan province, Viet Nam. He has worked closely with Dr. Thuan at Wireless Communications and Signal Processing Research Group at Industrial University of Ho Chi Minh City, Vietnam. He is currently pursue Master degree in field of wireless communications. His research interest includes electronic design, signal processing in wireless communications network, non- orthogonal multiple access, physical layer security.